Kohn-Sham potentials for fullerenes and spherical molecules

Y. Pavlyukh and J. Berakdar
Institut für Physik, Martin-Luther-Universität Halle-Wittenberg, Heinrich-Damerow-Strasse 4, D-06120 Halle, Germany
(Received 25 January 2010; published 22 April 2010)

We present a procedure for the construction of accurate Kohn-Sham potentials of quasispherical molecules starting from the first-principles valence densities. The method is demonstrated for the case of icosahedral $C_{20}{}^{2+}$ and C_{60} molecules. Provided the density is N representable the Hohenberg-Kohn theorem guarantees the uniqueness of the obtained potentials. The potential is iteratively built following the suggestion of R. van Leeuwen and E. J. Baerends [Phys. Rev. A **49**, 2421 (1994)]. The high symmetry of the molecules allows a parametrization of the angular dependence of the densities and the potentials using a small number of symmetry-adapted spherical harmonics. The radial behavior of these quantities is represented on a grid and the density is reconstructed from the approximate potential by numerically solving the coupled-channel Kohn-Sham equations. Subsequently, the potential is updated and the procedure is continued until convergence is achieved.

DOI: 10.1103/PhysRevA.81.042515 PACS number(s): 31.15.es, 31.15.A−

I. INTRODUCTION

The number of quantum-mechanical systems for which the electron density $n(\mathbf{r})$ is accurately known is quite limited. This is to be expected, as from $n(\mathbf{r})$ the ground-state total energy E_0 is deduced. In general E_0 can be numerically determined, for example, by using the expensive configuration interaction (CI) or coupled cluster (CC) methods. Even though these methods yield accurate E_0, a correct behavior of the obtained electron density cannot be taken for granted: in the asymptotic region ($r \to \infty$), where $n(\mathbf{r})$ decays as $\exp(-2\sqrt{2\varepsilon}r)$ [1] (ε is the lowest ionization potential), and also for $\mathbf{r} \to \mathbf{R}_a$ ($\mathbf{R}_a$ is any of the nuclei positions), where $n(\mathbf{r})$ is constrained by the nuclear cusp condition [2], an infinite number of Gaussian-type basis functions is needed to represent the density. Typically, however, only a small number of basis functions is optimized for the calculation in the valence region. Using Slater-type basis functions is a better choice in this respect, but even then best-known atomic densities have limited accuracy. For example, the widely used electronic density of Ne atoms computed by Bunge and Esquivel [3] has a relative error of 0.5% in the range $3 < r < 6$ bohrs, and the cusp condition is fulfilled with the same precision.

Systems with known accurate Kohn-Sham potentials are even a subset of the systems with known $n(\mathbf{r})$. The reason is that, although the Hohenberg-Kohn theorem [4] guarantees the uniqueness of the potential for a given $n(\mathbf{r})$ (there are also some exceptions [5]), it does not provide a mathematically straightforward prescription for its construction. On the other hand, to obtain $n(\mathbf{r})$ for a given potential one solves iteratively the Kohn-Sham equation with a given approximation for the exchange-correlation functional. For one- or two-electron systems the inverse problem can be solved exactly [6]. For many-electron systems this is still a daunting task [7–11].

This work is a contribution to fill partially this gap. We outline a prescription to construct accurate Kohn-Sham potentials for quasispherical molecules and illustrate the method for two prominent molecular systems, C_{60} and $C_{20}{}^{2+}$. These fullerenes are academically interesting and hold a promise for applications ranging from molecular electronics to quantum computing [12,13]. The vast majority of theoretical treatments dealing with these systems is based on a very crude approximation for the ionic and core electron potentials which results in the so-called jellium-shell model [14] with a spherically symmetric potential well of depth v_0 and width ΔR located at a distance R from the center of the molecule. The electrostatic potential of the valence electrons and the local density approximation for the exchange potential are self-consistently added, yielding a spherically symmetric Kohn-Sham potential. Despite its simplicity this model captures qualitatively the main features of the electronic structure; for example, it has been employed for the calculations of the Rydberg states [15], to study single and double ionization of C_{60} [16–24] and of $Ar@C_{60}$ [25], and to compute the fragmentation cross sections in He-C_{60} collisions [26,27].

Shortcomings of the model were recognized already by its inventors. Besides the poor treatment of electronic exchange and correlation, its elevated symmetry ($I_h \to O_3$) is the major source of errors. The most obvious consequence is the lack of electronic level splitting which results in the wrong prediction of 250 valence electrons instead of 240. A partial account for the icosahedral symmetry of the system was attempted by Yabana and Bertsch [28] in the same year that the jellium-shell model was proposed. However, components of the potential with angular momentum $\ell > 0$ were introduced as merely fitting parameters to obtain a spectrum in agreement with *ab initio* calculations. Here we numerically construct the Kohn-Sham potential starting from the *ab initio* electron density. We show that the density and the potential can be described by a small number of parameters, which is very advantageous computationally.

The outline of the article is as follows. In Sec. II we discuss the group theoretical properties of the I_h point symmetry and the representations of the group in terms of the spherical harmonics. The symmetry adapted functions composed of them form the basis for representations of the densities and the potentials. In Sec. III we analyze the valence density from the various quantum chemistry calculations. Further, we present details of our numerical method. It relies on the solution of the coupled-channel Schrödinger equation. We elaborate on aspects pertinent to angular momentum couplings and to the symmetry of the wave functions in Sec. IV. Finally, we present results for exchange-correlation potentials in Sec. V and conclude.

II. THE ICOSAHEDRAL POINT GROUP

The electron density and the exchange-correlation potential are the main quantities of interest for the present study. Exploiting the symmetry properties allows for an enormous simplification of their treatment. For spherical fullerenes, upon a proper or improper rotation, physical quantities transform according to the totally symmetric, one-dimensional representation (A_g) of the I_h symmetry group. The group contains 120 elements that can be constructed from four generators; it possesses one-dimesional (A_g,A_u), three-dimensional (T_{1g},T_{2g},T_{1u},T_{2u}), four-dimensional (G_g,G_u), and five-dimensional (H_g,H_u) representations [29]. On the other hand, the electronic density and the potential may be characterized by their angular momentum (ℓ) components [30]. To switch between these two points of view it is necessary to construct suitable linear combinations of the spherical harmonics $Y_{\ell,m}$ (i.e., the eigenfunctions of the angular momentum operators) that transform as the identity representation of the group I_h. We call these combinations *symmetry-adapted spherical functions* (SAFs). For the construction of SAFs one may use the projection operator method, its application to the I_h symmetry group is, however, extremely difficult. Motivated by applications in x-ray scattering and electron microscopy of viruses, in a number of studies SAFs were constructed for small ℓ. For $\ell \leqslant 30$ SAFs were tabulated by Prandl *et al.* [31]. The number of identity representations g_ℓ for each ℓ can be obtained from the generating function

$$\frac{1}{(x^6-1)(x^{10}-1)} = \sum_{\ell=0}^{\infty} g_\ell x^\ell.$$

There are only a few SAFs with low angular momentum ($\ell = 0, 6, 10, 12$), which is very attractive from a computational point of view. The density or the potential can be represented accurately up to the 12th order by just four functions. Staring from $\ell = 16$, SAFs with any even value of the angular momentum can be built; for $\ell = 30$, two one-dimensional representations appear for the first time ($g_{30} = 2$). Working with SAFs of such high orders is still a huge simplification; however, the coupling of the angular momenta given by the $3j$ symbols is numerically very demanding. Therefore, the numerical solution of the Kohn-Sham equation presented in this work is performed up to the order $\ell_m = 15$. The corresponding density has components up to the order 30.

In general, the electron density (same holds for the potential) can be represented as

$$n(\mathbf{r}) = \sum_{\ell=0}^{\infty} \sum_{\alpha_\ell=1}^{g_\ell} n_{\ell,\alpha_\ell}(r) I_{\ell,\alpha_\ell}(\theta,\phi). \tag{1}$$

Here $I_{\ell,\alpha_\ell}(\theta,\phi)$ denotes the symmetry adapted spherical function of ℓth order, index α_ℓ discriminates between different representations of the same angular momentum, and (r,θ,ϕ) are the spherical coordinates of the vector $\mathbf{r}$. The explicit expression for $I_{\ell,\alpha_\ell}(\theta,\phi)$ reads

$$I_{\ell,\alpha_\ell}(\theta,\phi) = \sum_{m=-\ell}^{\ell} \mathcal{I}^{(\alpha_\ell)}_{\ell,m} Y_{\ell,m}(\theta,\phi). \tag{2}$$

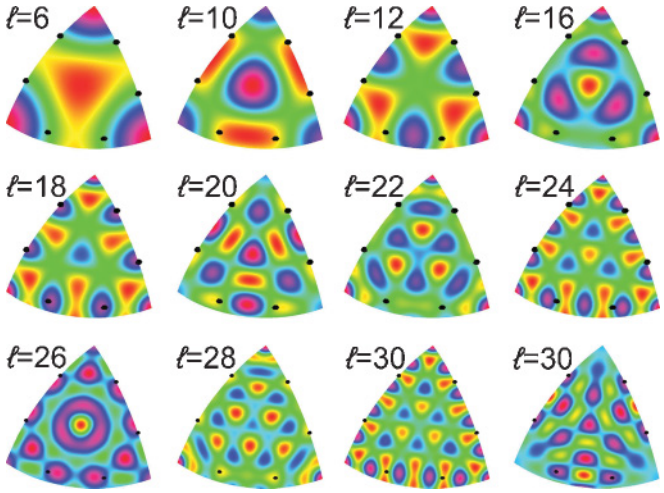

FIG. 1. (Color online) Symmetry-adapted spherical harmonics $I_{\ell,\alpha_\ell}(\theta,\phi)$ ($\ell = 6,\ldots,30$) coded by the hue color component. Due to the I_h symmetry it is sufficient to plot them only in a small irreducible domain of the spherical coordinate system. The spherical triangle $0 \leqslant \theta \leqslant \arccos(1/\sqrt{5})$, $0 \leqslant \phi \leqslant 2\pi/5$, containing six such domains is shown. Phases of the functions are selected as in [31]. The z axis is one of the fivefold axes. Black dots denote positions of the vertices of the truncated icosahedron. This idealized solid (all edges of the same length) is an almost perfect representation of the C_{60} fullerene (6-6 and 5-6 bond have slightly different lengths). At the center of the hexagon is situated a vertex of the dodecahedron, a solid representing the $C_{20}{}^{2+}$ molecule.

Apart from the trivial $I_{0,1}(\theta,\phi) = Y_{0,0}(\theta,\phi) = 1/\sqrt{4\pi}$, the simplest normalized SAF appears for $\ell = 6$:

$$I_{6,1}(\theta,\phi) = \tfrac{1}{5}[\sqrt{11}Y_{6,0} - \sqrt{7}(Y_{6,5} - Y_{6,-5})],$$

where we use the phase convention for the spherical harmonics $Y_{\ell,m}(\theta,\phi)$ as in [32] and the coordinate system is chosen such that the z axis is parallel to one of the axes of the fivefold symmetry and the y axis is parallel to one of the twofold axes. Some other SAFs are shown in Fig. 1.

Fast convergence is necessary for the expansion [Eq. (1)] to be useful for numerical computations; that is, only a few terms in Eq. (1) should accurately represent the quantity of interest. Let us consider at first the case of the *ionic potential*, $v^{(i)}(\mathbf{r})$. It can be analytically found by solving the Poisson equation with the ionic density $n^{(i)}(\mathbf{r})$. In our work we consider systems with N_a ionic sites having the same distance R to the center. For C_{60} we have $R = 3.568$ Å while for $C_{20}{}^{2+}$ we use $R = 2.03$ Å. Thus, the expansion of the ionic density is

$$\begin{aligned} n^{(i)}(\mathbf{r}) &= \sum_{a=1}^{N_a} q_{\text{ion}} \delta(\mathbf{r} - \mathbf{R}_a) \\ &= \frac{q_{\text{ion}} N_a}{\sqrt{4\pi}\, R^2} \delta(r - R) \sum_{\ell=0}^{\infty} \sum_{\alpha_\ell=1}^{g_\ell} C^{(i)}_{\ell,\alpha_\ell} I_{\ell,\alpha_\ell}(\theta,\phi). \end{aligned} \tag{3}$$

Here q_{ion} is the charge of the ion ($q_{\text{ion}} = 6$ for carbon atoms). By writing the density in such a form we set the first expansion

coefficient $C_{0,1}$ to one. The ionic potential can be found from the spherical Bessel transforms of the density; that is,

$$v_\ell^{(i)}(r) = 4\pi \frac{2}{\pi} \int_0^\infty dq \tilde{n}_\ell^{(i)}(q) j_\ell(qr), \tag{4a}$$

$$\tilde{n}_\ell^{(i)}(q) = \int_0^\infty dr' r'^2 n_\ell^{(i)}(r') j_\ell(qr'), \tag{4b}$$

where $j_\ell(x)$ denotes the spherical Bessel function. In this work we adopt atomic units. In these notations the Poisson equation reads $\Delta v^{(i)}(\mathbf{r}) = -4\pi n^{(i)}(\mathbf{r})$. For

$$n_\ell^{(i)}(r) = \frac{q_{\text{ion}} N_a}{\sqrt{4\pi} R^2} C_{\ell,\alpha_\ell}^{(i)} \delta(r - R),$$

all integrals are performed analytically (Eq. 6.512.1 of [33]) with the result

$$v_\ell^{(i)}(r) = q_{\text{ion}} N_a \sqrt{4\pi} \frac{C_{\ell,\alpha_\ell}^{(i)}}{2\ell + 1} \times \begin{cases} \dfrac{r^\ell}{R^{\ell+1}} & \text{for } r \leqslant R, \\ \dfrac{R^\ell}{r^{\ell+1}} & \text{for } r > R. \end{cases} \tag{5}$$

The singularity of $v^{(i)}(\mathbf{r})$ at $\mathbf{r} = \mathbf{R}_a$ does not appear in the radial functions $v_\ell^{(i)}(r)$. They are continuous for all values of r and have a finite peak (removable singularity) at $r = R$. Away from the shell, already the second radial function $v_6^{(i)}(r)$ decays very fast. Thus, apart from the disturbance at $r = R$ components of the ionic potential with higher angular momenta have little influence on the electron density. However, as will be shown subsequently, all of them contribute substantially to the potential at $r = R$. In other words, the expansion coefficients $C_{\ell,\alpha_\ell}^{(i)}$ are slowly decaying functions of ℓ.

The coefficients $C_{\ell,\alpha_\ell}^{(i)}$ can be computed as a sum over the spherical coordinates (θ_a, ϕ_a) of the atoms,

$$C_{\ell,\alpha_\ell}^{(i)} = \frac{\sqrt{4\pi}}{N_a} \sum_{a=1}^{N_a} I_{\ell,\alpha_\ell}(\theta_a, \phi_a), \tag{6}$$

or as a limit of the following spherical integral,

$$C_{\ell,\alpha_\ell}^{(i)} = \frac{\sqrt{4\pi}}{N_a} \lim_{\varepsilon \to 0} \int d\Omega\, I_{\ell,\alpha_\ell}(\theta,\phi) \sum_{a=1}^{N_a} \delta_\varepsilon(\Omega_a - \Omega), \tag{7}$$

where $\Omega_a = (\theta_a, \phi_a)$ denote the atomic positions in the spherical coordinate system, and δ_ε represents some numerical regularization of the δ function on the sphere, that is, $\lim_{\varepsilon \to 0} \delta_\varepsilon(\Omega) = \delta(\Omega)$. To obtain the last equation we used the identity

$$\sum_{a=1}^{N_a} \delta(\mathbf{r} - \mathbf{R}_a) = \delta(r - R) \sum_{a=1}^{N_a} \delta(\Omega_a - \Omega).$$

Typical representation for the three-dimensional δ function is

$$\delta(\mathbf{r} - \mathbf{R}_a) = \lim_{\sigma \to 0} \frac{1}{(\sqrt{2\pi}\sigma)^3} \exp\left[-\frac{(\mathbf{r} - \mathbf{R}_a)^2}{2\sigma^2} \right].$$

If $R_a = R$ in a spherical coordinate system [$\mathbf{r} = (r, \Omega)$ and $\mathbf{R}_a = (R, \Omega_a)$], we have

$$\delta(\mathbf{r} - \mathbf{R}_a) = \delta(r - R) \lim_{\varepsilon \to 0} \frac{1}{(\sqrt{2\pi}\varepsilon)^2 R^2} \exp\left[-\frac{|\Omega - \Omega_a|^2}{2\varepsilon^2} \right],$$

where $|\Omega - \Omega_a|$ denotes the distance between the points on the unit sphere. Note, the integrals in Eq. (7) are nonuniform functions of the regularization parameter ε. Therefore, in practice, Eq. (6) is preferred. However, the density still is expressible in a form suitable for numerical analysis:

$$n^{(i)}(\mathbf{r}) = \frac{q_{\text{ion}}}{R^2} \delta(r - R) \lim_{\varepsilon \to 0} \frac{1}{(\sqrt{2\pi}\varepsilon)^2} \times \exp\left[-\frac{1}{2\varepsilon^2} \sum_{\ell=0}^{\infty} \sum_{\alpha_\ell=1}^{g_\ell} \zeta_{\ell,\alpha_\ell}^{(i)} I_{\ell,\alpha_\ell}(\theta,\phi) \right]. \tag{8}$$

This relation resembles the cumulant expansions in statistical physics or probability theory. Hence, we call it the *cumulant expansion of the density in terms of SAF*. The expansion coefficients $\zeta_{\ell,\alpha_\ell}^{(i)}$ are computed by a formula analogous to Eq. (7):

$$\zeta_{\ell,\alpha_\ell}^{(i)} = \int d\Omega\, I_{\ell,\alpha_\ell}(\theta,\phi) \hat{n}_\varepsilon^{(i)}(\theta,\phi), \tag{9}$$

$$\hat{n}_\varepsilon^{(i)}(\theta,\phi) = -2\varepsilon^2 \log\left[\sum_{a=1}^{N_a} \exp\left(-\frac{|\Omega_a - \Omega|^2}{2\varepsilon^2} \right) \right]. \tag{10}$$

In contrast to the density $n^{(i)}(\mathbf{r})$, its regularizations $\hat{n}_\varepsilon^{(i)}(\theta,\phi)$ on the sphere are smooth functions of angles which are independent of the regularization parameter ε provided it is small. Equation (9) is thus suitable for numerical integration. By comparing Eqs. (3) and (8) we find

$$\frac{N_a}{\sqrt{4\pi}} \sum_{\ell=0}^{\infty} \sum_{\alpha_\ell=1}^{g_\ell} C_{\ell,\alpha_\ell}^{(i)} I_{\ell,\alpha_\ell}(\theta,\phi) = \lim_{\varepsilon \to 0} \frac{1}{(\sqrt{2\pi}\varepsilon)^2} \exp\left[-\frac{1}{2\varepsilon^2} \sum_{\ell=0}^{\infty} \sum_{\alpha_\ell=1}^{g_\ell} \zeta_{\ell,\alpha_\ell}^{(i)} I_{\ell,\alpha_\ell}(\theta,\phi) \right]. \tag{11}$$

Furthermore, we introduce coefficients

$$\zeta_\ell^{(i)} = \sqrt{\sum_{\alpha_\ell=1}^{g_\ell} \left| \zeta_{\ell,\alpha_\ell}^{(i)} \right|^2}.$$

Their magnitude serves as an indicator for truncating the SAF expansion, Eq. (1). We depicted the coefficients for all five regular polyhedra and for the truncated icosahedron (idealization for the C_{60} fullerene) in Fig. (2). As expected from the smoothness of the regularized ionic density $\hat{n}_\varepsilon^{(i)}(\theta,\phi)$, $\zeta_\ell^{(i)}$ are well-behaved functions of ℓ that algebraically decay for $\ell \to \infty$. This decay is, however, not monotonic; the coefficients may rather be grouped into several series (with uniform convergence) reflecting the peculiarity of the geometric structure. In the context of two prototypical molecules we observe three distinct series for $C_{20}{}^{2+}$ ($\{6n\}$, $\{6n + 10\}$, $\{6n + 20\}$) and five series for C_{60} ($\{10n\}$, $\{6, 10n + 12\}$, $\{18, 10n + 24\}$, $\{16, 28, 10n + 36\}$, $\{26, 10n + 38\}$), where $n = 0, \ldots$. To describe correctly the ionic density and the potential at least the first term of each series is necessary, meaning that for $C_{20}{}^{2+}$ terms up to $\ell = 20$ are required, while for C_{60} inclusion of contributions up to $\ell = 28$ is necessary. Up to now we considered only the ionic density and the

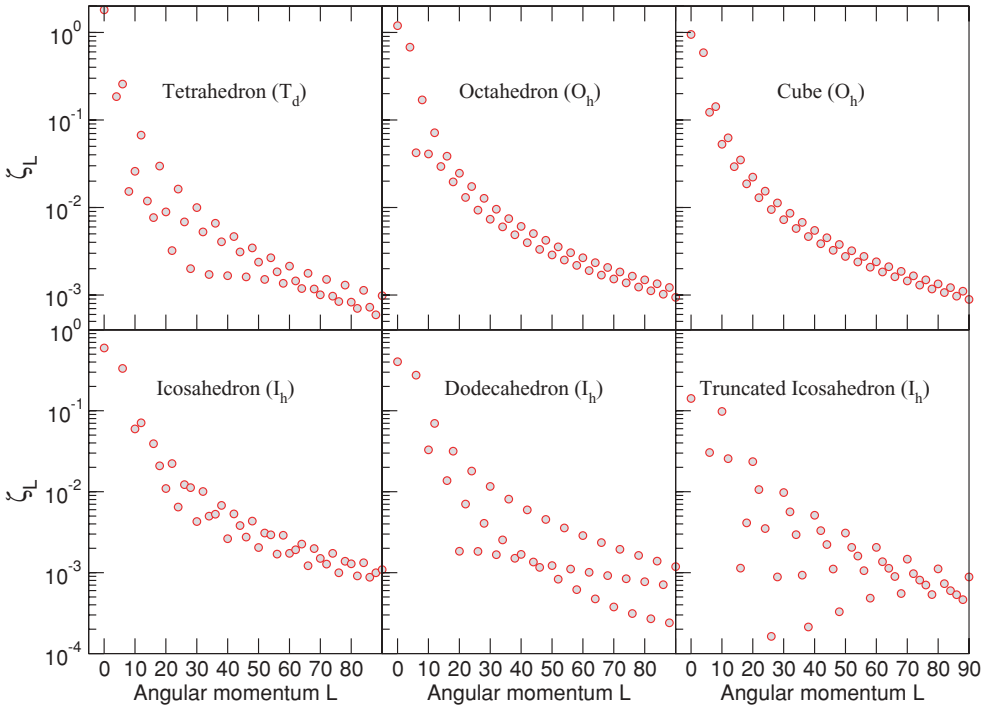

FIG. 2. (Color online) Expansion coefficients $\zeta_\ell^{(i)}$ for five regular polyhedra and for the truncated icosahedron.

corresponding potential. Core electrons are localized close to the nuclei; therefore they require similar treatment. In contrast, the valence electrons are much more delocalized. Their description can be much more accurate with a smaller number of terms.

III. ELECTRONIC DENSITIES

The electron densities, an input for the inverse problem, were obtained from the full-electron and pseudopotential quantum chemistry calculations with the GAUSSIAN 03 [34] package. We used the 6-311++G($2d$,$2p$) basis set [35] **(**(12s,6p,2d)/[5s,4p,2d] contraction scheme**)** for the full-electron calculations, and the pseudopotential calculations were performed using the CRENBL basis set [36] (4s4p uncontracted scheme). The densities were computed on a grid in real space and subsequently projected on the SAFs for each radial point of the spherical coordinate system.

$$n_{\ell,\alpha_\ell}(r) = \int d\Omega\, n(\mathbf{r}) I_{\ell,\alpha_\ell}(\theta,\phi). \tag{12}$$

The choice of the coordinate system is important here. The molecules in *ab initio* calculations were oriented as shown in Fig. 3, that is, with the twofold axis aligned along the z axis. Since the SAFs tabulated in [31] are given in a different orientation they must be rotated. The rotation of SAFs of the order ℓ is accomplished by applying the Wigner D function to the vector of length $2\ell+1$ containing the coefficients of the SAF expansion:

$$\tilde{\mathcal{I}}_{\ell,m'}^{(\alpha_\ell)} = \sum_{m=-\ell}^{\ell} \mathcal{I}_{\ell,m}^{(\alpha_\ell)} D_{mm'}^{\ell}(\alpha,\beta,\gamma).$$

The Wigner functions can be expressed via the Jacobi polynomials **(**$P_s^{(\mu,\nu)}(x)$**)**:

$$D_{mm'}^{\ell}(\alpha,\beta,\gamma) = e^{-im\alpha} d_{mm'}^{\ell}(\beta) e^{im'\gamma},$$

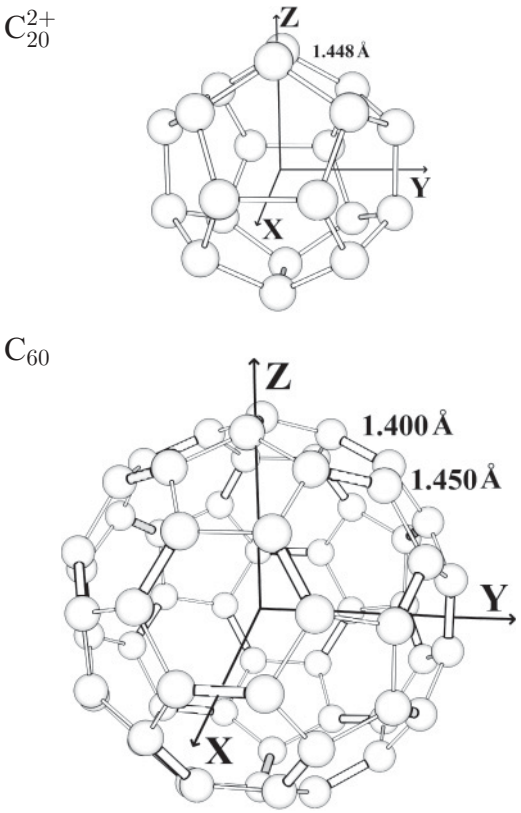

FIG. 3. Geometric structure and orientation of the studied molecules.

$$d^{\ell}_{mm'}(\beta) = \xi_{mm'}\sqrt{\frac{s!(s+\mu+\nu)!}{(s+\mu)!(s+\nu)!}},$$
$$\times\left(\sin\frac{\beta}{2}\right)^{\mu}\left(\cos\frac{\beta}{2}\right)^{\nu}P_s^{(\mu,\nu)}(\cos\beta),$$
$$\xi_{mm'} = \begin{cases} 1 & \text{for } m' \geqslant m, \\ (-1)^{m'-m} & \text{for } m' < m, \end{cases}$$
$$\mu = |m-m'|, \quad \nu = |m+m'|, \quad s = \ell - \tfrac{1}{2}(\mu+\nu).$$

For the molecule's orientation the angles are $\gamma = 0$,

$$\beta = \arccos\left(\sqrt{\frac{5+\sqrt{5}}{10}}\right),$$

and $\alpha = 0$ for C_{60} and $\alpha = \frac{\pi}{2}$ for $C_{20}{}^{2+}$, where the β angle is the angle between the twofold and fivefold symmetry axes. The accuracy of the expansion, Eq. (12), is assessed by computing the relative error

$$\epsilon = \frac{1}{q_{\text{ion}}N_a}\int_0^{\infty} r^2 dr \int d\Omega \left| n(\mathbf{r}) - \sum_{\ell=0}^{\ell_m}\sum_{\alpha_\ell=1}^{g_\ell} n_{\ell,\alpha_\ell}(r) I_{\ell,\alpha_\ell}(\theta,\phi)\right|. \tag{13}$$

At large distances from the nuclei the density decays erroneously as $\exp(-kr^2)$ as a result of using Gaussian-type orbitals (GTO). To circumvent this issue we extrapolated the density tails with the $\exp(-\kappa r)$ function. For our calculation we found it sufficient to consider radial distances in the range up to 6 Å for $C_{20}{}^{2+}$ and to 8 Å for C_{60}; 900 and 1200 radial points were used, respectively. It is important, especially for large ℓ, to have an accurate algorithm for performing angular integrations, Eq. (12). The Lebedev integrators, typically used in density functional codes, are designed to accurately integrate spherical harmonics up to a certain order. In these applications the center of the sphere where the integration is performed is located on the nucleus. This guarantees the smoothness of the electron density and makes the method well suited for quantum chemical calculations. In contrast to these applications, the origin of the spherical coordinate system in the present work coincides with the center of the molecule and is not situated on the nucleus. When the sphere of integration crosses the nuclei the integrated function is not smooth any more and contains contributions of infinite order in ℓ. This renders the Lebedev method impractical. Besides being able to integrate peaked functions there are several further requirements for our desired quadrature. One should be able to gradually vary the number of integration points in order to check the convergence of integrals and, thus, to assess the accuracy of the computational scheme. The grid should be uniform and isotropic. And, finally, there should be a fast and simple algorithm to generate weights and grid coordinates. In all these respects we found the "Fibonacci grids" introduced by Hannay and Nye [37] to have clear advantages over the conventional Lebedev grids. The number of integration points is $N = 2f_n$, where f_n denotes the nth Fibonacci number, while the error scales as N^{-6}. We use grids with different numbers of angular points (n ranging from 18 to 22) depending on the vicinity of the integration sphere to the nuclei.

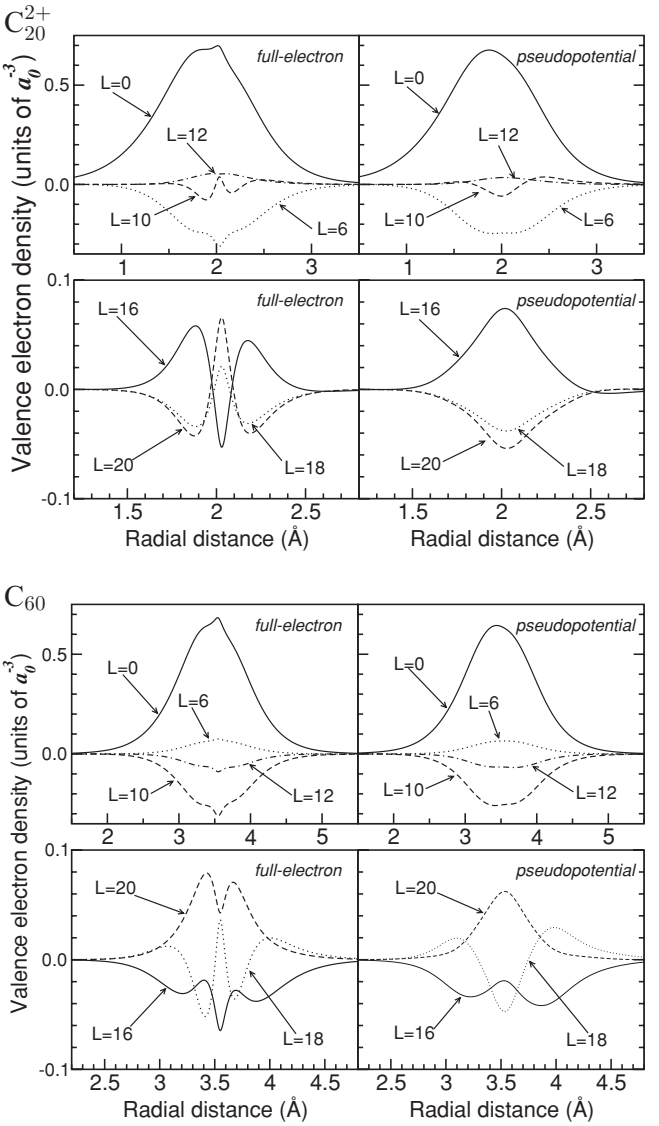

FIG. 4. Electron density of the studied molecules. Left vs right panels compare the Hartree-Fock valence density from full-electron vs pseudopotential calculations.

At first we discuss the low angular momentum components of the valence electron density shown in Fig. 4. The densities from the full-electron calculations are sharply peaked at the radius of the geometric shell. In contrast, the corresponding densities from the pseudopotential calculations are more smooth and the maximum of the angular averaged ($\ell = 0$) density is slightly shifted toward the center of the molecule. The angular-averaged densities of two systems are very similar; for $C_{20}{}^{2+}$ it is slightly more extended into the inner region. The second largest components, as anticipated from Figs. 1 and 2, are $\ell = 6$ and $\ell = 10$ for smaller and larger shells, respectively. By including only the first three terms in the expansion, Eq. (12), the relative error is 8% for full-electron and 6% for pseudopotential densities. If terms up to and including $\ell = 30$ are added, the relative error is further reduced to 2% and 0.5%, respectively.

A nonlocal or, in most applications semilocal, operator of the pseudopotential eliminates the core-electron states. Due

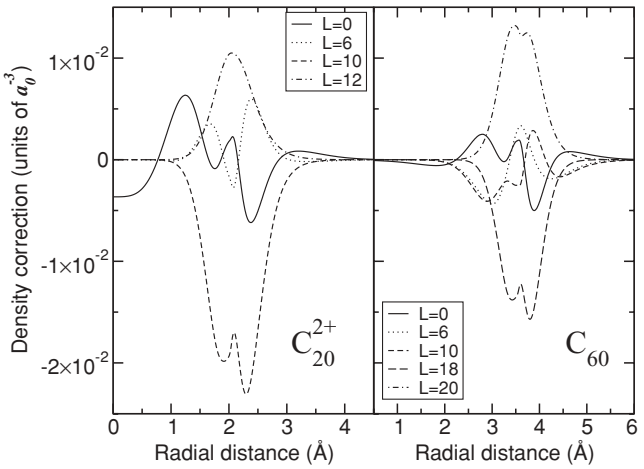

FIG. 5. The difference of valence densities from the Hartree-Fock and MP_2 methods.

to the oscillation theorem, the lowest valence states from the pseudopotential calculation are inevitably nodeless. Hence, the use of pseudopotentials reduces the number of nodes in the density expansion; the effect is seen for the density components $\ell \geqslant 10$ for $C_{20}{}^{2+}$ and for $\ell \geqslant 16$ for C_{60}.

Up to now we have considered valence electron densities from the Hartree-Fock method which yields the single-particle states and serves as a basis for subsequent correlated calculations. For the smaller system we succeeded in obtaining the densities via the coupled-cluster singles and doubles (CCSD) method. For the C_{60} fullerene we applied the MP_2 perturbation theory which is known to provide total energies, bond lengths, and reaction barriers with accuracy comparable to (or often better than) the best density-functional methods. The CCSD method is more precise, but is computationally demanding. It is often superseded in accuracy by the CCSD(T), the gold standard of quantum chemistry. However, the latter is not suitable for our purposes since it can only provide the total energy and not the density. Large improvement of the total energies provided by the correlated methods requires minimal changes in the total electron density. This is evidenced by Fig. 5 where the dominant density differences of the Hartree-Fock and MP_2 methods are plotted. The error introduced by the truncation of the angular expansion often exceeded the difference between the Hartree-Fock and correlated densities. Therefore, if not explicitly stated, we use for the analysis the Hartree-Fock density and the corresponding potential.

From the shown results, several routes to accurate exchange-correlation potential for fullerenes seem appropriate: Ideally, the electron density from the most precise correlated method based on the *full-electron* calculation should be used. This would require a solution of the Kohn-Sham equation with a trial potential for very high values of the angular momentum on each iteration step; that is, large-ℓ components are needed to obtain the core states. Our aim is, however, to represent the potential by just a few angular components to make it attractive for use by other researchers for other purposes. If the potential expansion [Eq. (5)] is truncated at low ℓ, the potential at the nuclei position may well be too shallow to support bound core states. An efficient way to find the Kohn-Sham potential is to perform all the computations using localized basis functions for the expansion of the potential. At the present time these methods are still too computationally demanding. In this work we take advantage of the fact that the valence electron density from the pseudopotential calculations is a smooth function that requires only a small number of symmetry adapted functions for its expansion.

Let us assume for a moment that we solve the inverse problem and have found the corresponding local Kohn-Sham potential. Because it is constructed from the valence electron density it is tempting to say that the potential can be separated into local and nonlocal parts. To the first group belongs (i) the Hartree potential of the valence electrons and (ii) the interaction with the nuclei. The nonlocal part contains (i) the exchange and the correlation potential of the valence electrons and (ii) the pseudopotential. This last term models the effect of the core electrons. We note that for alkali metals the nonlocal core correction is significant and must be accounted for. For carbon, however, this effect is minor. In the calculations one uses typically a semilocal expression for the pseudopotential that acts differently on the s and p and higher projections of the wave functions. The exchange-correlation potential and the pseudopotential are two nonlocal terms formally incorporated in the *local* Kohn-Sham potential. Considerable effort has been devoted to the development of accurate approximations for either part. Would it be possible to estimate these quantities from the computed Kohn-Sham potential? Because they are both nonlocal this is formally not possible. If, however, one takes into account that the nonlocal part of the pseudopotential is strongly localized on the nuclei, already at $r \approx 0.8$ Å the pseudopotential is indistinguishable from Z_{core}/r for carbon, and we can still find the exchange-correlation potential from our calculation.

IV. COUPLED-CHANNEL SCHRÖDINGER EQUATION

The basic component of our approach is the numerical solution of the Schrödinger equation on a grid. Since we expand the potential, the wave functions, and the densities in terms of the spherical harmonics the three-dimensional eigenvalue problem is reduced to one dimension for the radial functions. Our potential is angular dependent, that is, we consider terms beyond $\ell = 0$. Hence, the coupling between the components of wave functions are to be treated which implies a solution of *the coupled-channel Schrödinger equation*. The numerical solution is far more demanding than for the ordinary 1D equation: In contrast to the single-channel case, the presence of degenerate eigenstates poses a problem. Fortunately, each eigenstate can still be characterized by a unique generalized node count. This follows from the generalization of the oscillation theorem to the multichannel case. The number can be used to classify the states and to differentiate states that are accidentally close to each other (they have a different number of nodes) from truly degenerate states with the same number of nodes. In application to fullerenes, this is extremely important since the states are densely spaced and almost always degenerate.

There are several methods available to tackle this problem [38–40]. For the calculations we used our implementation of the renormalized Numerov method [38,41], widely used in studies of molecular vibrations, etc. For details, we refer the

reader to the original article. Here we recapitulate the main features of the method. For the maximal angular momentum ℓ_m there are $n_m = (\ell_m + 1)^2$ coupled equations and wave-function components. Generally speaking, they are complex-valued functions. However, since we do not involve magnetic fields, the wave functions can all be selected to be real without loss of generality.

For a test value of the eigenenergy the propagation is performed from the left and from the right edges of the interval to a matching point. The eigenvalue ε_n with generalized node number n_n is said to be converged if the lower and the upper energy limits ($\varepsilon_L \leqslant \varepsilon_n < \varepsilon_U$) are found such that

$$|\varepsilon_L - \varepsilon_U| < h,$$
$$N(\varepsilon_L) = n_n < N(\varepsilon_U),$$

where h is the tolerance typically set to 10^{-10} and $N(\varepsilon)$ denotes the number of nodes for energy ε solution. The tolerance h sets also a threshold between two closely spaced groups of states or a single degenerate state. After the state has been converged $N(\varepsilon_U) - N(\varepsilon_L)$ yields its degeneracy. Each propagation step requires two $n_m \times n_m$ symmetric matrix inversions. This constitutes the main computational cost. Thus, the method scales as $n_r \ell_m^6$, where n_r is the number of radial grid points. A node-counting algorithm is used to calculate degenerate eigenstates and to indicate their degeneracy. In the case of a few nondegenerate states appearing for $\ell = 0$ and $\ell = 6$ we used the faster Brent method after the eigenvalue had already been isolated; that is, ε_L, and ε_U are found with $N(\varepsilon_U) - N(\varepsilon_L) = 1$. Otherwise, we are using the bisection procedure.

Since the numerical cost of the method steeply increases with maximal angular momentum we decided not to work with complex-valued wave functions excluding all redundant components. Thus, by solely working with real functions we can achieve 8 times speedup at the cost of more complicated algorithms for coupling different angular momentum components. Let us focus now on that part of the Hamiltonian containing this coupling.

Its matrix elements in the complex case are easily expressed via the product of two Wigner $3jm$ symbols (cf. Eq. 5.9.5 of [32]), namely,

$$\begin{aligned}\langle \ell_1, m_1 | Y_{\ell,m} | \ell_2, m_2 \rangle &= \int Y^*_{\ell_1,m_1} Y_{\ell,m} Y_{\ell_2,m_2} d\Omega \\ &= (-1)^{m_1} \sqrt{\frac{(2\ell_1+1)(2\ell+1)(2\ell_2+1)}{4\pi}} \\ &\quad \times \begin{pmatrix} \ell_1 & \ell & \ell_2 \\ 0 & 0 & 0 \end{pmatrix} \begin{pmatrix} \ell_1 & \ell & \ell_2 \\ -m_1 & m & m_2 \end{pmatrix}. \end{aligned} \tag{14}$$

One can also express them in terms of a single Gaunt coefficient.

Real functions are expandable in terms of spherical harmonics as

$$f(\theta,\phi) = \sum_{\ell=0}^{\ell_m} \left[a_{\ell,0} Y_{\ell,0}(\theta,\phi) + \sqrt{2} \sum_{m=1}^{\ell} \mathrm{Re}[a_{\ell,m} Y_{\ell,m}(\theta,\phi)] \right].$$

For each ℓ there are $2\ell + 1$ *normalized real* basis functions which can be selected in the form $Y_{\ell,0}$, $\sqrt{2}\mathrm{Re}Y_{\ell,m}$, $\sqrt{2}\mathrm{Im}Y_{\ell,m}$ ($m > 0$). Integrals containing products of three such functions [in analogy with Eq. (14)] can be cast as a linear combination of the Gaunt coefficients. However, the final equations are quite cumbersome, for one needs to treat differently three kinds of real basis functions. For our calculations a large number of the Gaunt coefficients of high order are necessary. They were precomputed with the MATHEMATICA symbolic algebra package and stored.

Upon the nth step all occupied Kohn-Sham (KS) eigenstates $\psi_i(\mathbf{r})$ are computed with some approximate KS potential $v_s^{(n)}(\mathbf{r})$. Then we calculate the electron density

$$n_{\mathrm{KS}}^{(n)}(\mathbf{r}) = 2 \sum_{i=1}^{N_e} |\psi_i(\mathbf{r})|^2 \tag{15}$$

and apply the van Leeuwen iterative procedure to obtain the update of the KS potential,

$$v_s^{(n+1)}(\mathbf{r}) = \frac{n_{\mathrm{ref}}(\mathbf{r}) + \alpha}{n_{\mathrm{KS}}^{(n)}(\mathbf{r}) + \alpha} v_s^{(n)}(\mathbf{r}). \tag{16}$$

The constant α is used to stabilize the recursion. Note, we apply the recursion to the total potential and not to the electron-repulsion part as in [9] (see also the remark on the fourth page of [10]). The density contains expansion coefficients with the maximal angular momentum $2\ell_m$. They are computed analytically from the wave-function expansion coefficients using the Clebsh-Gordon algebra. To obtain the expansion coefficients for the potential, Eq. (16) is represented on a mesh in real space and projected onto the SAFs by performing the angular integration [as in Eq. (12)].

The iterative refinement of the potential as outlined still needs to be refined for fullerenes. The problems of the numerical stability of such an algorithm have already been observed and discussed in [10]. They even appear in the case of a *single Ne atom*. One aspect, already brought to the attention by these authors, is the sensitivity of the method to the initial guess of the potential. Apart from that, in the case of fullerenes one faces another challenge related to the computation of the KS density. If at some point in the iterative process the potential acquires angular distribution slightly different from the searched one, this will, most probably, lead to an incorrect sequence of electronic states. For instance, in the case of $C_{20}{}^{2+}$ there is a competition between the h_u, t_{1u}, and t_{2u} states (13 states of $\ell = 6$ symmetry split in the I_h environment into one five-dimensional and two three-dimensional multiples) to be occupied. According to the Hartree-Fock calculation only h_u should be occupied. In the course of calculation it frequently appears that the substates' order is reverted. If so, the electron density computed from such (partially occupied states) has different symmetry from the target density. As a consequence, if such unphysical density is used to update the potential it will only amplify the initial error, and the potential will never converge. In addition, one would need some prescription for how to deal with partially filled states. As a simple solution, one might think of introducing some fractional occupation numbers. We found that this does not work either because the resulting density does not transform according to A_g representation. The only way to obtain reliable results and to have stable iterations is, in our opinion, to determine the electron configuration in each iteration step and to assign the

occupation numbers according to the electron configuration from the Hartree-Fock method [42]. For the systems of interest they are summarized as

$$\mathrm{C}_{20}{}^{2+}: \underbrace{a_g}_{0}\ \underbrace{t_{1u}}_{1}\ \underbrace{h_g}_{2}\ \underbrace{g_u\,t_{2u}}_{3}\ \underbrace{g_g}_{4}\ \underbrace{a_g}_{0}\ \underbrace{h_g}_{4}\ \underbrace{h_u}_{5}\ \underbrace{t_{1u}}_{1}\ \underbrace{h_g}_{2},$$

$$\mathrm{C}_{60}: \underbrace{a_g}_{0}\ \underbrace{t_{1u}}_{1}\ \underbrace{h_g}_{2}\ \underbrace{t_{2u}\,g_u}_{3}\ \underbrace{h_g\,g_g}_{4}\ \underbrace{h_u\,t_{1u}\,t_{2u}}_{5}\ \underbrace{t_{1g}\,h_g\,a_g\,g_g}_{6}$$
$$\underbrace{h_u\,t_{1u}\,t_{2u}}_{7}\ \underbrace{a_g}_{0}\ \underbrace{g_u}_{7}\ \underbrace{h_g}_{8}\ \underbrace{t_{1u}}_{1}\ \underbrace{g_g\,t_{2g}}_{8}\ \underbrace{g_u}_{9}\ \underbrace{h_g}_{2}$$
$$\underbrace{h_g}_{8}\ \underbrace{h_u}_{9}\ \underbrace{t_{2u}\,g_u}_{3}\ \underbrace{g_g\,h_g}_{4}\ \underbrace{h_u}_{5},$$

where the dominant ℓ value is shown below each symmetry class. They were determined with the help of multiplet-splitting tabulated in [43].

In our work we found it sufficient to analyze the electronic configuration in a simplified way. Thus, we determine the symmetry properties of each eigenstate with respect to SO(3) rather than the I_h group symmetry operations. This amounts to assigning to each wave function a set of probabilities $\{s_\ell\}$ to be in the ℓ angular momentum state. The state n is said to have the angular momentum ℓ_n if the corresponding number is maximal. If all components of the potential with $\ell > 0$ were zero, the system would possess a spherical symmetry and such a classification would be exact ($s_\ell = 1$ for ℓ angular momentum state, otherwise zero). Realistically, the potential always introduces some symmetry breaking. This results in level splitting and in an admixture of other angular momentum components. We found that such an angular momentum analysis together with the information on the degeneracy (from the Numerov method) can be used to unambiguously classify the states. Thus, Eq. (15) is modified to include only the states with the correct symmetry and degeneracy into the density.

V. RESULTS

In Sec. III we gave a description of the electron densities of fullerenes studied. In Sec. IV we established a numerical method for solving the Schrödinger equation with a trial angular-dependent local potential and presented details of the iterative procedure leading to the Kohn-Sham potential associated with the target density (obtained from the *ab initio* pseudopotential calculations). The pseudopotential density has been selected as being better suited for our method. It is free from oscillations in the core region and, thus, can be represented by a small number of angular components. To the best of our knowledge the pseudopotential density is used here for the first time as a target for the inverse Kohn-Sham problem. Therefore, one might question the very existence of the local Kohn-Sham potential yielding such a density. As we mentioned previously, the pseudopotential for the carbon atom is a semilocal operator,

$$w(\mathbf{r},\mathbf{r}') = w_{\mathrm{local}}(r) + \delta(r-r') \times \sum_{\ell} \Delta w_\ell(r) \sum_{m=-\ell}^{\ell} Y^*_{\ell m}(\hat{r}') Y_{\ell m}(\hat{r}).$$

The s and p pseudopotentials for carbon are very distinct functions. Several schemes for the generation of pseudopotentials are reviewed, and real and Fourier space dependencies are analyzed by Troullier and Martins [44]. Typically, the s channel is a more shallow function at the origin than the p channel.

The Hohenberg and Kohn theory cannot be applied directly to systems with nonlocal external potential. According to their mathematical proof [4], the existence of a unique local Kohn-Sham potential is only guaranteed for the v-representable density, that is, a density that is associated with an antisymmetric ground-state wave function of some Hamiltonian with local external potential. The theorem proven by Levy [45] extends the validity domain of the Hohenberg-Kohn theory to N-representable densities, that is, functions that may be obtained from some antisymmetric many-body wave function. Thus, the restriction on the external potential to be local can safely be omitted. The N-representability condition is rather weak and easily satisfied by a trial n. The theorem of Levy is the foundation of our method. However, one issue has to be discussed: On the one hand we state that the pseudopotential for carbon must be nonlocal, while on the other hand the Kohn-Sham potential yielding the same density as pseudopotential calculations is local. This is similar to ambiguity arising when considering the exchange operator. Despite the fact that the actual nature of this operator is nonlocal, one can still construct the corresponding local Kohn-Sham potential. The method to do so belongs to the realm of the optimized effective potential (OEP) approach. The nonlocal expression is generally valid, including the system with a trial density during the self-consistency loop. Independently, the *local* potential can be constructed, but only for the true density.

We seek an initial approximation to the sought potential. The jellium-shell potential of Puska and Nieminen [14] allows for a fine-tuning of the state energies by adjusting a few parameters. The initial approximation has the form of two Heaviside step functions:

$$v^{(0)}_{s\,\ell=0}(r) = \sqrt{4\pi}U \times \left[\theta_\delta\left(r - R + \frac{\Delta}{2}\right) - \theta_\delta\left(r - R - \frac{\Delta}{2}\right)\right],$$
$$\theta_\delta(x) = \frac{1}{2\pi i}\left[\log(x - i\delta) - \log(-x - i\delta)\right], \qquad (17)$$

where U and Δ denote the depth and the width of the potential well, and we introduced a small parameter δ ($0.2a_0$ for C_{60} and $0.1a_0$ for $\mathrm{C}_{20}{}^{2+}$) in order to allow for the potential to decay algebraically away from the shell. This facilitates the convergence in the regions where the potential is small. We deliberately selected a different initial depth and width of the potential well in order to demonstrate the independence of the converged results on the initial parameters (Fig. 6).

For comparison, we also show the electrostatic potential and exchange potential from the local density approximation:

$$v_x^{(\mathrm{LDA})}(\mathbf{r}) = -\left(\frac{3}{\pi}n(\mathbf{r})\right)^{1/3}.$$

The electrostatic potential includes the Hartree potential of the valence electrons and the ionic potential. Since we exclude the core electrons from consideration the ionic charge is set

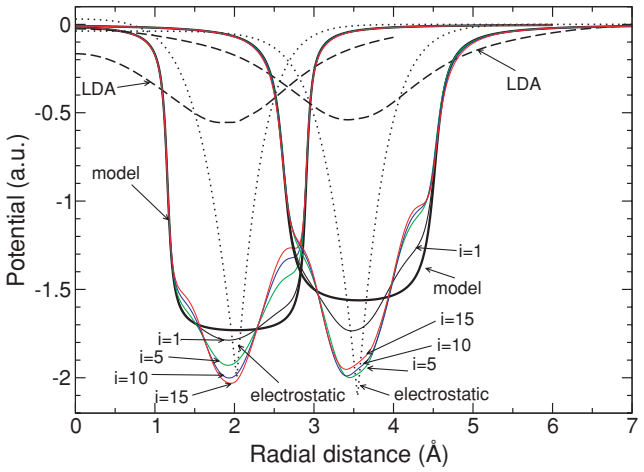

FIG. 6. (Color online) Spherically averaged potentials ($\ell = 0$ component multiplied by $1/\sqrt{4\pi}$) for $C_{20}{}^{2+}$ and C_{60} systems. The thick solid line denotes the Puska and Nieminen model potentials [14] according to Eq. (17) parametrization. The dotted and dashed lines denote the electrostatic and LDA exchange potential corresponding to the target density. The thin lines denote the Kohn-Sham potential v_s in the course of iterative optimization.

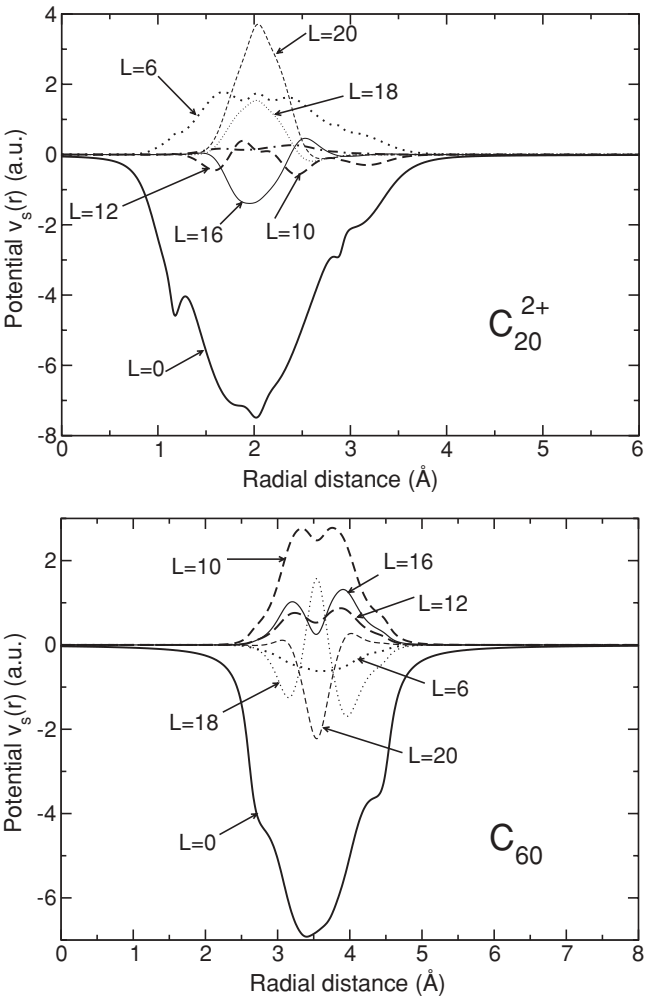

FIG. 7. The Kohn-Sham potentials.

to 4. The electrostatic potential is computed by numerically solving the Poisson equation by two spherical Bessel transforms [Eqs. (4a) and (4b)]. The details are presented in the Appendix.

The converged Kohn-Sham potentials are depicted in Fig. 7. We used here the pseudopotential Hartree-Fock density as a target. The calculations were performed for $\ell_m = 15$. Let us consider separately two aspects of the obtained potentials: (i) the angular dependence and (ii) the radial dependence. Contrary to widespread opinion, the deviation of the potential from spherical symmetry is substantial and is not identical to the angular dependence of the density. For the $C_{20}{}^{2+}$ molecule, the density is characterized by a large $\ell = 6$ term, while the potential is dominated by an $\ell = 16$ contribution. It is interesting to observe that if we had perturbatively taken $\ell > 10$ potential terms into account, they would lead to vanishing energy correction for all occupied states in this system. This follows from the fact that all occupied states have angular momentum $\ell \leqslant 5$. The high-ℓ components of the potential can still affect the states via the second-order energy corrections. For C_{60} they are also important; however, the $\ell = 10$ term is large for both the density and the potential. The occurrence of large angular momentum terms in the potential is an important message of the present work. It shows a limited character of the model calculations with spherically symmetric potentials. The limitations cannot be surmounted by the use of perturbation theory because the second-order treatment formally requires the summations to be performed over all states, including the unoccupied ones.

Also the radial behavior of the $\ell = 0$ potentials differs considerably from the model potentials [14,28]. In order to understand the details one can single out the exchange-correlation part ($v_{\rm xc}$) of the Kohn-Sham potential and further partition it into several components as is done in [46] and references therein,

$$v_{\rm xc} = v_{\rm xc}^{\rm hole} + v_{c,\rm kin} + v^{\rm resp}.$$

Here we make only some qualitative remarks: The intershell peaks are a well-established feature of $v_{\rm xc}$ and were noticed for numerous atomic systems. For the carbon atom Morrison and Zhao [47] found intershell peaks at around 0.3 Å from the nucleus. They are typically attributed to the stark variation of $v_{c,\rm kin}$ in the region between $1s$ and $2s$ or $2p$ shells. The intershell peaks are well differentiated from the comparably large potential oscillations at the core region when the target density is taken from the GTO calculations [48]. There are several reasons why the potential oscillation in our systems is much less pronounced. One aspect is that there are no contributions to the kinetic potential $v_{c,\rm kin}$ from the "interaction" between the core and valence states. Furthermore, our density is rather smooth in the core region due to the use of pseudopotential. As for the origin of the two asymmetric peaks at around 0.7 Å on both sides of the shell we recall the findings of Schipper *et al.* [48]: Using a method based on the linear response theory they were able to achieve the convergence much faster than with the van Leeuwen method. This increased the accuracy of the potential and reveals unphysical features

often masked by convergence problems of the slower method. Due to the complexity of our system it was not possible to perform 10 000 iterations to obtain fully convergent results. At most 100 iterations could be performed. However, as noted in [48], a fair picture of the potential is feasible at this number of iterations. Furthermore, already at this point the relative error computed according to Eq. (13) is comparable with the error of the target density due to the truncation of the SAF expansion. Hence, we do not converge the potential to a better accuracy than that of the given density.

It is possible to evaluate the $v_{c,\mathrm{kin}}$ part of v_{xc} explicitly and to verify if this term is responsible for the small peaks in the potential. This part is given as the difference between the kinetic potential computed on the true many-body (v_{kin}) and the single-determinant many-body function constructed from the Kohn-Sham orbitals ($v_{s,\mathrm{kin}}$). In its general form it is expressed in terms of the nonlocal two-particle density matrix. However, for the case of the single determinantal wave functions it is reduced to [49]

$$v_{s,\mathrm{kin}}(\mathbf{r}) = \frac{1}{2}\sum_{i=1}^{N_e}\left|\frac{\nabla\phi_i(\mathbf{r})}{\sqrt{n(\mathbf{r})}}\right|^2. \tag{18}$$

Several studies of kinetic terms are known ([46] and references therein). They were evaluated from the Hartree-Fock orbitals [50] and from the many-body functions [51]; $v_{c,\mathrm{kin}}$ was computed from the optimized potential model [52]. For the case of Hartree-Fock target densities, $v_{c,\mathrm{kin}}$ is given as the difference of the kinetic potentials computed on the Hartree-Fock and Kohn-Sham orbitals [Eq. (18) can be used in both cases]. Since the difference between these orbitals is rather small, we argue that the kinetic term alone cannot be responsible for the peak.

VI. CONCLUSIONS

We presented a method for the construction of the Kohn-Sham potential for quasispherical molecules and illustrated the method by calculations for two representative spherical fullerenes. The density from the pseudopotential calculations was used as a target for the inverse problem. Large magnitudes of high angular momentum components and complicated radial dependence indicate strong deviations of the potential from known models. The calculations can be viewed as a starting point for more systematic investigations of the exact Kohn-Sham potentials for fullerenes. We envisage several extensions in terms of densities: (i) more accurate densities from the Slater-type orbital expansions, (ii) densities from full-electron calculations rather than from pseudopotential calculations, and (iii) correlated densities. Only alternative (i) is easily realized with our methodology. The others require inclusion of even higher angular momentum components. This is mandatory for a correct description of the core states. One also needs a better accuracy for the density in order to appreciate the role of electronic correlations. From the methodological view, there are other possibilities to solve the inverse problem. More sophisticated methods can provide the same accuracy with a smaller number of iterations. However, only methods which rely on localized basis functions for the expansion of the potentials can independently verify the real space results.

Theoretical study of photoionization of fullerenes is one of the possible applications of the constructed potentials. Considerations based on the acceleration form of the dipole operator can be used to unveil dominant contributions to photoionization. For the case of the jellium-shell model, theory predicts four oscillation frequencies related to the spatial regions with a large potential gradient [53]. These oscillations were indeed observed in experiment [54]. However, certain features in the Fourier transform of the partial photoionization cross section can only be explained with the use of realistic potentials.

APPENDIX: NUMERICAL SOLUTION OF THE POISSON EQUATION

We comment briefly on the solution of the Poisson equation with respect to the numerical problems that may arise when using a brute force approach. Such an implementation scales as n_r^2. A possible approach utilizes one of the several methods relying on the fast Fourier transformation (FFT) [55,56] (scale as $n_r \log_2 n_r$). A disadvantage here is the use of logarithmic grids. Recently, a FFT-based method with a uniform grid was proposed [56]. These methods are quite involved and do not automatically guarantee accurate results if the function to be transformed is oscillating and/or slowly decaying at infinity. Since these two conditions simultaneously occur for the second transform [Eq. (4a)] we developed another approach. It provides very accurate results for the potentials at the cost of n_r^2 scaling. The method is based on two observations: (i) the electron density is strongly localized at and decays exponentially away from the shell radius, and (ii) the direct transform for the ionic density can be computed analytically and subtracted from the numerical transform of the electron density. From the first observation it follows that the first improper integral can be replaced by the integration in finite limits without any loss of accuracy. For its numerical evaluation we use the Filon method (see Sec. 2.10.2 of [57]). In the original formulation the method is applied to integration of products involving trigonometric functions, for example,

$$I(k) = \int_a^b f(t)\left\{\begin{matrix}\cos kt\\ \sin kt\end{matrix}\right\} dt.$$

It can be also used for spherical Bessel transforms since these functions can be expressed as a combination of sine and cosine functions. We use this previously unexploited fact to devise the following expression:

$$\begin{aligned}\int_a^b j_\ell(qr)f(r)\,dr &\approx h\{\beta C_{2n} + \gamma C_{2n-1}\\ &\quad + \alpha[f(b)y_\ell(qb) - f(a)y_\ell(qa)]\}\\ C_{2n} &= \frac{1}{2}f(a)j_\ell(qa) + f(a+2h)j_\ell(q(a+2h))\\ &\quad + f(a+4h)j_\ell(q(a+4h)) + \cdots + \frac{1}{2}f(b)j_\ell(qb),\\ C_{2n-1} &= f(a+h)j_\ell(q(a+h)) + f(a+3h)j_\ell(q(a+3h))\\ &\quad + \cdots + f(b-h)j_\ell(q(b-h)),\end{aligned}$$

where $y_\ell(z)$ is the spherical Bessel function of the second kind, h is the integration step, and the coefficients α, β, and γ are the

same as in Filon's method. The integration interval is divided into two parts, in the small interval close to the origin ($[0,a]$) we use the Simpson method because $y_\ell(z)$ functions are diverging there. The Filon method is used for larger values of r. The transition point a is selected at the middle between the first zero of the $j_\ell(qr_1^{(j)}) = 0$ and $y_\ell(qr_1^{(y)}) = 0$ functions, that is,

$$a = \tfrac{1}{2}\left(r_1^{(j)} + r_1^{(y)}\right).$$

The second transform yielding the potential [Eq. (4a)] is applied to an oscillating and slowly decaying function proportional to the q-dependent density. In general one would need some sophisticated methods for its integration. However, since we subtract the analytic transform of the ionic density prior to the transform, the function becomes more localized in q space. The effect of slowly decaying tails can be eliminated in a controlled way by increasing the interval of integration. We found very accurate results for the number of q points $n_q = 16n_r$ and the interval of integration $[0,q_m]$, where $q_m = 12n_r/r_m$. The integration is performed with the Simpson method.

[1] J. Katriel and E. R. Davidson, Proc. Natl. Acad. Sci. USA **77**, 4403 (1980).
[2] E. Steiner, J. Chem. Phys. **39**, 2365 (1963).
[3] A. V. Bunge and R. O. Esquivel, Phys. Rev. A **34**, 853 (1986).
[4] P. Hohenberg and W. Kohn, Phys. Rev. **136**, B864 (1964).
[5] M. Levy, Phys. Rev. A **26**, 1200 (1982).
[6] C. O. Almbladh and A. C. Pedroza, Phys. Rev. A **29**, 2322 (1984).
[7] F. Aryasetiawan and M. J. Stott, Phys. Rev. B **38**, 2974 (1988).
[8] Q. Zhao, R. C. Morrison, and R. G. Parr, Phys. Rev. A **50**, 2138 (1994).
[9] R. van Leeuwen and E. J. Baerends, Phys. Rev. A **49**, 2421 (1994).
[10] K. Peirs, D. Van Neck, and M. Waroquier, Phys. Rev. A **67**, 012505 (2003).
[11] E. S. Kadantsev and M. J. Stott, Phys. Rev. A **69**, 012502 (2004).
[12] M. S. Dresselhaus, G. Dresselhaus, and P. C. Eklund, *Science of Fullerenes and Carbon Nanotubes* (Academic Press, San Diego, 1996).
[13] W. Harneit, M. Waiblinger, K. Lips, C. Meyer, A. Weidinger, and J. Twamley, in *Proceedings of the 1st International Conference on Experimental Implementation of Quantum Computation*, edited by R. G. Clark (Rinton Press, Princeton, 2001).
[14] M. J. Puska and R. M. Nieminen, Phys. Rev. A **47**, 1181 (1993).
[15] M. Boyle, K. Hoffmann, C. P. Schulz, I. V. Hertel, R. D. Levine, and E. E. B. Campbell, Phys. Rev. Lett. **87**, 273401 (2001).
[16] A. Rüdel, R. Hentges, U. Becker, H. S. Chakraborty, M. E. Madjet, and J. M. Rost, Phys. Rev. Lett. **89**, 125503 (2002).
[17] S. W. J. Scully *et al.*, Phys. Rev. Lett. **94**, 065503 (2005).
[18] M. E. Madjet, H. S. Chakraborty, J. M. Rost, and S. T. Manson, J. Phys. B **41**, 105101 (2008).
[19] A. K. Belyaev, A. S. Tiukanov, A. I. Toropkin, V. K. Ivanov, R. G. Polozkov, and A. V. Solov'yov, Phys. Scr. **80**, 048121 (2009).
[20] O. Kidun and J. Berakdar, Phys. Rev. Lett. **87**, 263401 (2001).
[21] O. Kidun and J. Berakdar, Surf. Sci. **507**, 662 (2002).
[22] O. Kidun, N. Fominykh, and J. Berakdar, Chem. Phys. Lett. **410**, 293 (2005).
[23] O. Kidun, N. Fominykh, and J. Berakdar, J. Phys. B **37**, L321 (2004).
[24] O. Kidun, D. Bauer, N. Fominykh, and J. Berakdar, J. Phys. B: At. Mol. Opt. Phys. **40**, 4617 (2007).
[25] M. E. Madjet, H. S. Chakraborty, and S. T. Manson, Phys. Rev. Lett. **99**, 243003 (2007).
[26] T. Schlathölter, O. Hadjar, R. Hoekstra, and R. Morgenstern, Phys. Rev. Lett. **82**, 73 (1999).
[27] A. Rentenier *et al.*, Phys. Rev. Lett. **100**, 183401 (2008).
[28] K. Yabana and G. F. Bertsch, Phys. Scr. **48**, 633 (1993).
[29] D. B. Litvin, Acta Crystallogr. A **47**, 70 (1991).
[30] Y. Pavlyukh and J. Berakdar, Chem. Phys. Lett. **468**, 313 (2009).
[31] W. Prandl, P. Schiebel, and K. Wulf, Acta Crystallogr. A **52**, 171 (1996).
[32] D. A. Varshalovich, A. N. Moskalev, and V. K. Khersonskii, *Quantum Theory of Angular Momentum* (World Scientific, Singapore, 1988).
[33] I. S. Gradstein and I. M. Ryzhik, *Table of Integrals, Series, and Products* (Academic Press, San Diego, 2007), 7th ed.
[34] M. J. Frisch *et al.*, GAUSSIAN03, Revision C.02 (Gaussian, Inc., Pittsburgh, PA, 2003).
[35] M. J. Frisch, J. A. Pople, and J. S. Binkley, J. Chem. Phys. **80**, 3265 (1984).
[36] L. F. Pacios and P. A. Christiansen, J. Chem. Phys. **82**, 2664 (1985).
[37] J. H. Hannay and J. F. Nye, J. Phys. A: Math. Gen. **37**, 11591 (2004).
[38] B. R. Johnson, J. Chem. Phys. **69**, 4678 (1978).
[39] J. M. Hutson, Comput. Phys. Commun. **84**, 1 (1994).
[40] S. A. Chin, S. Janecek, and E. Krotscheck, Chem. Phys. Lett. **470**, 342 (2009).
[41] B. R. Johnson, J. Chem. Phys. **67**, 4086 (1977).
[42] In general, the Hartree-Fock occupation numbers might deviate from the occupations of the Kohn-Sham orbitals. This takes place when the Hartree-Fock method converges to an excited state of the system, which, nonetheless, is the true stable ground state in the Hartree-Fock sense. Such a situation can occur for weakly bound systems with numerous low-energy excited states. For spherical fullerenes this scenario is rather improbable due to the high symmetry and high stability of these molecules.
[43] K. Shirai, J. Phys. Soc. Jpn. **61**, 2735 (1992).
[44] N. Troullier and J. L. Martins, Phys. Rev. B **43**, 1993 (1991).
[45] M. Levy, Proc. Natl. Acad. Sci. USA **76**, 6062 (1979).
[46] E. J. Baerends and O. V. Gritsenko, J. Phys. Chem. A **101**, 5383 (1997).
[47] R. C. Morrison and Q. Zhao, Phys. Rev. A **51**, 1980 (1995).
[48] P. R. T. Schipper, O. V. Gritsenko, and E. J. Baerends, Theor. Chem. Acc. **98**, 16 (1997).
[49] M. Levy and H. Ou-Yang, Phys. Rev. A **38**, 625 (1988).
[50] A. Sierraalta and E. V. Ludeña, Int. J. Quantum Chem. **30**, 277 (1986).
[51] M. A. Buijse, E. J. Baerends, and J. G. Snijders, Phys. Rev. A **40**, 4190 (1989).

[52] O. Gritsenko, R. van Leeuwen, and E. J. Baerends, J. Chem. Phys. **101**, 8955 (1994).
[53] O. Frank and J. M. Rost, Chem. Phys. Lett. **271**, 367 (1997).
[54] A. Rüdel, R. Hentges, U. Becker, H. S. Chakraborty, M. E. Madjet, and J. M. Rost, Phys. Rev. Lett. **89**, 125503 (2002).
[55] J. D. Talman, Comput. Phys. Commun. **30**, 93 (1983).
[56] M. Toyoda and T. Ozaki, Comput. Phys. Commun. **181**, 277 (2010).
[57] P. J. Davis and P. Rabinowitz, *Methods of Numerical Integration (Computer Science and Applied Mathematics)* (Academic Press, San Diego, 1984), 2nd ed.